

## Analytical Study of Conjugated Heat Transfer of a Microchannel Fluid Flow between Two Parallel Plates

A. S. Al-shyyab<sup>1\*</sup>, F. H. Darwish<sup>1</sup>, M. A. Al-Nimr<sup>2</sup>, and B. J. Alshaer<sup>2</sup>

<sup>1</sup>*Aeronautical Engineering Department, Jordan University of Science and Technology, Irbid, 22110 Jordan*

<sup>2</sup>*Mechanical Engineering Department Jordan University of Science and Technology, Irbid, 22110 Jordan*

Received September 4, 2018; in final form, December 25, 2019; accepted January 9, 2020

**Abstract**—The conjugated temperature distributions of a microchannel fluid flow between two semi-infinite parallel plates are obtained analytically. The variables separation and transformation techniques are implemented to introduce the degenerate hypergeometric differential equation, the solution of which is given in terms of Kummer's functions. The eigenvalues of the corresponding transcendental characteristic equation are obtained using a mathematical solver software package. Non-dimensional analysis of the governing equations introduced the parameter of “solid-fluid heat conduction ratio”  $k_k$ . Values of this parameter are considered to present two limiting case solutions, namely, the adiabatic boundary solution, when  $k_k \approx 0$  and the isothermal boundary solution, when  $k_k > 100$ . The Nusselt number  $Nu$  of the two limiting solutions is obtained and compared accurately with the corresponding values from the literature. The effect of the Knudsen number  $Kn$ , the Biot number  $Bi$ , and the conductivity ratio  $k_k$  on the temperature, temperature jump, and the Nusselt number is investigated. It is found that the temperature jump near the flow entrance becomes more significant with increase in  $Kn$ ,  $Bi$ , or  $k_k$ . On the other hand, the Nusselt number is found to increase with growing  $Kn$  and decrease with increasing  $Bi$  or  $k_k$ .

**DOI:** 10.1134/S1810232820010099

### INTRODUCTION

The inevitable use of the technological high-power dissipative microelectronic chips in miniaturized and microelectromechanical systems (MEMS) has implicitly demanded good understanding of the conjugated thermal behavior of essential thermal management components such as rectangular microchannels with relatively high geometric aspect ratios. A few examples in this regard include the use of microchannel cooling system in concentrator photovoltaics with cell micro-solar collectors. In such applications, a well-designed cooling system helps to increase the efficiency of energy conversion of photovoltaic cells. Microchannel cooling systems are also used to enhance the performance of special-use batteries during rapid charging and discharging, which deteriorates at elevated temperatures. Micro spacing of three-dimensional stacking chips warrants microchannel paths, which are convenient for forced convection cooling when printed circuit boards are considered as microchannel walls. In such devices, the micro space between the stacked boards cannot accommodate thermal spreaders for effective cooling. This justifies the implementation of forced convection in such devices. Last but not least, micro heat tubes and pipes are considered to be the most effective means of cooling high heat flux density sources, where micro channels are used as condensers, evaporators, and superheated vapor and/or liquid carrying paths.

The thermal and hydrodynamical behavior of flow inside microchannels depends on the value of the Knudsen number, which is defined as the ratio of the molecular mean free path  $\lambda$  to the channel characteristic length  $L$ . Accordingly, a gaseous flow in a channel can be generally classified into four types. Type I is the conventional macrochannel flow regime in which the channel characteristic length is

\*E-mail: asalshyyab@just.edu.jo

larger than  $200 \mu\text{m}$  or equivalently  $Kn < 0.001$ . The conventional continuum approach coupled with the no-slip/no-jump condition at the solid-fluid interface can be adopted to model the thermal and hydrodynamic behaviors of this flow type. Type 2 is the microchannel slip flow regime in which the channel characteristic length is within  $200 \sim 10 \mu\text{m}$ , which is considered to be a few orders of magnitude of the Knudsen layer thickness ( $0.001 < Kn < 0.1$ ). The continuum approach can be adopted as in Type 1 to model the flow behavior, but with consideration of the slip/jump condition at the solid-fluid interface in order to allow for the gas rarefaction. Either the continuum approach coupled with the second order slip/jump condition or the free-molecular flow model can be adopted in Type 3, the transitional flow regime, which is characterized by  $0.1 < Kn < 10$ . Finally, Type 4 is the free molecular flow regime in which  $Kn > 10$ . In this case, the continuum approach breaks down and the molecular kinetic-based model must be adopted.

Historically, hydrodynamically fully developed and thermally developing laminar incompressible forced-convection heat transfer in macrochannel ducts is known as the Graetz problem. Graetz and Nusselt independently solved this problem analytically nearly hundred years ago [1–3]. In their solutions, neither the streamwise axial conduction nor the flow viscous dissipation was considered. Since then, this problem has been explored extensively through several studies, in which the viscous dissipation and/or the streamwise axial conduction were considered for fluid flows inside different geometric channels. Shah [4] conducted a comprehensive review of the solutions described by the Graetz problem and its extensions.

The advent of MEMS and the relevant microchannel flow enticed researches in the last decades to reiterate Graetz and similar problems, yet extended to include the velocity slip and temperature jump conditions at the solid-fluid interface, inherent to microchannel flows in the slip flow regime. Mikhailov and Cotta [5] provided an analytic solution for a slip flow inside a parallel plate microchannel. They transformed the energy equation to the hypergeometric confluent equation. The corresponding eigenfunctions were found analytically in terms of confluent hypergeometric functions. Mathematica notebook was used to numerically solve the eigenvalues. The temperature profile of the flow was constructed using these eigenfunctions.

The microchannel Graetz problem was also extended to include axial conduction and viscous dissipation. Jeong and Jeong [6] analyzed the Graetz problem of hydrodynamically fully developed and thermally developing fluid flow in the slip flow regime. The flow microchannel was composed of semi-infinite flat plates. The viscous dissipation and the flow axial heat conduction were included. The velocity and temperature distributions, as well as the Nusselt number, were determined analytically for two different types of boundary conditions: constant heat flux and isothermal walls. Aydın and Avcı [7] considered a thermally developing but hydrodynamically fully developed micro-tube flow, where the effect of viscous dissipation was included in the formulation. Their study included the determination of the velocity and temperature profiles, as well as the Nusselt number.

Çetin et al. [8] used the eigenfunction expansion to determine the temperature profile and the Nusselt number in terms of confluent hypergeometric functions for an internal flow of micro-tubes in which the viscous dissipation and axial conduction terms were considered in the formulation. Aydın and Avcı [9, 10] and Avcı and Aydın [11] analyzed a similar problem of microchannel flows with consideration of both hydrodynamically and thermally fully developed flow for two types of isothermal and constant heat flux boundary conditions with viscous dissipation terms included. P. Lee and S.V. Garimella [12] considered three-dimensional rectangular microchannel flows of different aspect ratios and proposed generalized correlations for the Nusselt number as a function of the flow axial distance and channel aspect ratio.

Kuddusi and Egrican [13] and Kuddusi [14] employed an integral transform for the non-dimensional momentum and energy equations of a rectangular microchannel flow. Rarefaction effects are introduced into the problem by first-order slip/jump conditions. The solutions in the transformed domain are inverted to the physical domain of the problem by applying the transform inversion formula. They obtained the flow velocity and temperature distributions for eight combinations of constant temperature and adiabatic boundary walls of the channel. The Nusselt number they calculated agreed well with certain cases of data available in the literature. In a later work, Kuddusi and Cetegen [15] employed the mathematical similarity between the governing equations of two-dimensional heat conduction of non-uniform heat generations and the non-dimensional governing equations of flow inside a rectangular microchannel.

The analytic solution for the conduction problem is used to obtain the microchannel flow temperature distributions by replacing the parameters of the conduction problem with the mathematically corresponding parameters of the microchannel flow. Their analysis covers eight combinations of channel boundary walls subject to constant heat flux and adiabatic walls. Sadeghi and Saidi [16] obtained closed-form solutions for the velocity and temperature distributions, as well as the entropy generation for a rarefied gaseous flow confined between two parallel plates of asymmetric heat fluxes. Baghani et al. [17] extended the classical theoretical studies of a flow within a macrochannel of constant cross-section and arbitrary shape to allow for the boundary rarefaction effects of gaseous flow within microchannels. They have developed semi-analytic solutions in conjunction with the least squares optimization criterion to impose the H1 boundary conditions.

Rij et al. [18] numerically evaluated the effects of viscous dissipation of rectangular microchannel flows on the Nusselt number by using a computational fluid dynamics algorithm with slip-velocity and temperature-jump boundary conditions. Their numerical results for the limiting case of parallel plate flow agreed well with the analytic solutions. Mahulikar et al. [19] incorporated the effects of variable microflow thermophysical parameters and neglected the gas rarefaction effects in their analysis in order to address the significance of the variations of these thermophysical parameters on the pressure drop and friction factors.

The microchannel boundary wall thickness was neglected in all these studies, although it was comparable with the characteristic length (hydraulic diameter) and has a considerable effect on the thermal behavior of the system. Solutions of conjugate heat transfer problems that combine both convection and conduction heat transfer modes provide results that are more accurate. Therefore, the effects of wall thickness on the thermal behavior of the microchannel flow problems were taken into account. Conjugated macro scale heat transfer problems were investigated extensively using analytical, numerical, or experimental methods [20–30]. Conjugated heat transfer problems of microchannel flows gained increased interest in the last decade due to the bigger density of power dissipating electronic and MEMS devices.

K.K. Ambatipudi and M.M. Rahman [31] developed a model of numerical simulation for conjugated heat transfer and fluid flow in an array of rectangular microchannels. They have examined the effects of the channel aspect ratio, number of channels, and Reynolds number on the thermal performance. The numerical results they obtained agreed well with the experimental results conducted by Harms [32]. Zhang et al. [33] investigated the effects of axial heat transfer and the pipe wall thickness on the conjugate heat transfer of straight circular pipe. Increase in the wall-to-fluid conduction ratio for all values of aspect ratio less than 25 provided a uniform heat flux to the wall.

Nonino et al. [34] used a hybrid FEM that adapted the step-by-step solution of parabolized momentum equations in the fluid domain, which are used to solve the energy equation in the entire solid and fluid domains of simultaneously developing pipe flow. They investigated the effects of the axial heat conduction in the wall, the solid-fluid conductivity ratio, the solid wall thickness, and the micro-tube length on the local values of the Nusselt number and the fluid bulk temperature, as well as the wall axial temperature distributions. They concluded that the Nusselt number decreases with increase in the wall thickness or the conduction ratio and decreases as the pipe length lessens. Avcı et al. [35] investigated the combined effects of the solid-to-fluid conduction ratio and the viscous dissipation of various length-to-diameter ratios of micro-tube internal laminar flow. Kabar et al. [36] investigated the effects of rarefaction, axial conduction within the solid wall and fluid flow, and the development of both hydrodynamic and thermal boundary layers of rectangular microchannel flow subject to H1 boundary conditions. The thermo-fluid system governing equations were solved using the finite volume technique.

The aforementioned studies and investigations of microchannel flow considered microflows within different geometric cross-section channels and various preset boundary conditions of special cases of heat transfer. To the best knowledge of the authors of this research, none of the available literature studies considered the conjugated heat transfer of gaseous flow between two micro-spaced semi-infinite parallel plates (a microchannel with a high aspect ratio of  $> 25$ ) subjected to forced convection prescribed by the ambient temperature and the convection heat transfer coefficient values. This gap in the literature and the fact that practical high-aspect-ratio microchannel flows can be approximated by a flow between two semi-infinite parallel plates are the motives of this research. Hence, the aims of this research is to analytically obtain the temperature solutions within a gaseous flow between two micro-spaced semi-infinite parallel plates and within the plates themselves by adopting the continuum approach coupled

with the slip/jump condition at the solid-fluid interface. The outer surfaces of the boundary walls are subject to the general case of forced convection characterized by the Biot number and the ambient temperature. In addition, the study aim is to investigate the effect of the thermal and momentum parameters on the temperature solutions, the solid-fluid interface temperature-jump, and the Nusselt number.

### MATHEMATICAL MODEL

A steady-state pressure-driven rarefied gas flow between two semi-infinite parallel plates is considered in this study. The plates are separated by a micro-distance  $2H$  as shown in Fig. 1. The external surfaces of the plates are subjected to forced convection characterized by given values of the Biot number  $Bi$ . The channel environment is of the ambient temperature  $T_\infty$ . The fluid is assumed to be a hydrodynamically fully developed and thermally developing Newtonian incompressible one-dimensional laminar flow. Its thermal conductivity is  $k_f$ . The thermal conductivity of the isotropic material plates is  $k_s$ . The thickness of each plate  $\bar{t}$  covers the domain  $|H| < |z| < |\bar{W}|$ , i.e.,  $\bar{t} = |\bar{W} - H|$ . Therefore, the plane at  $z = 0$  is a plane of symmetry. The fluid enters the channel with a uniform temperature  $T_i$  and decays downstream. For small values of the Knudsen number ( $0.001 < Kn < 0.1$ ), the rarefied gas flow behavior can be described by the principles of continuum mechanics subject to slip/jump-boundary conditions. Using the rectangular coordinates, the momentum equation is expressed as follows:

$$\frac{\partial^2 u}{\partial z^2} = \frac{-1}{\mu} \left| \frac{\partial p}{\partial x} \right|, \quad 0 < z < H, \quad x > 0, \quad (1)$$

where  $x$  is the axial location measured from the inlet cross-section,  $z$  is the flow transverse direction measured from the flow center plane,  $u$  is the fluid velocity profile in the flow axial direction,  $\mu$  is the viscosity, and  $p$  is the static pressure.

The symmetrical velocity profile suggests that

$$\left. \frac{\partial u}{\partial z} \right|_{z=0} = 0, \quad (2)$$

at the flow centerline, whereas, neglecting the thermal creep, the first-order slip-velocity boundary conditions at the plate inner surface, at  $z = H$  are as follows:

$$u(H) = -\beta_v \lambda \left. \frac{\partial u}{\partial z} \right|_{z=H}, \quad 0 < x; \quad (3)$$

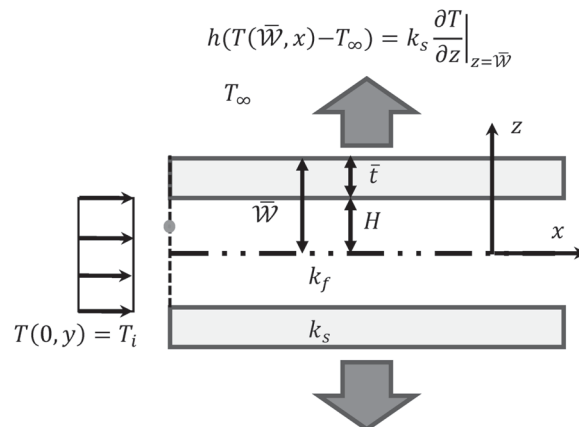


Fig. 1. Sketch of microchannel rarefied gas flow.

here  $\beta_v = (2 - \sigma_v)/\sigma_v$ , where  $\sigma_v$  is the tangential-momentum accommodation factor, its value for most engineering applications approaching 0.8, and  $\lambda$  is the molecular mean free path.

The heat conduction in the solid walls and the flow is two-dimensional. However, for simplicity, the axial heat conduction in the plates and the flow is considered to be negligible. Besides, the flow viscous dissipation is considered to be negligible as well, and thus the flow conservation of energy equation can be written as follows:

$$\rho_f c_f u \frac{\partial T_f}{\partial x} = k_f \frac{\partial^2 T_f}{\partial z^2}, \quad 0 < |z| < H, \quad 0 < x. \quad (4)$$

Similarly, the wall temperature distribution  $T_s$  is governed by the following equation:

$$\frac{\partial^2 T_s}{\partial z^2} = 0, \quad H < |z| < \bar{W}, \quad (5)$$

where  $T_f$  and  $T_s$  are the temperature distributions in the fluid flow domain  $0 < |z| < H$  and the boundary domain  $H < |z| < \bar{W}$ , respectively;  $\rho_f$ ,  $c_f$ , and  $k_f$  are the density, specific heat, and heat conduction coefficient of the flow, respectively.

The distribution of the flow temperature at the channel entrance is uniform and thus

$$T_f(0, z) = T_i, \quad x = 0, \quad 0 < z < H, \quad (6)$$

and it is symmetrical in the  $z$  direction of the entire domain. Therefore,

$$\left. \frac{\partial T_f}{\partial z} \right|_{z=0} = 0, \quad 0 \leq x. \quad (7)$$

The wall boundaries at the fluid-solid interface have a temperature-jump discontinuity described by the following expression:

$$T_f(x, H) - T_s(x, H) = -\beta_T \lambda \left. \frac{\partial T_f(x, z)}{\partial z} \right|_{z=H}, \quad 0 \leq x. \quad (8)$$

The parameter  $\beta_T$  meets the expression  $\beta_T = 2\gamma(2 - \sigma_T)/(\sigma_T \text{Pr}(\gamma + 1))$ , where  $\sigma_T$  is known as the thermal accommodation factor and  $\gamma$  and  $\text{Pr}$  are the specific heat ratio and the Prandtl number of the flow, respectively. Further, the heat flux through the inner fluid-solid interface imposes another boundary condition:

$$\left. \frac{\partial T_f(x, z)}{\partial z} \right|_{z=H} = k_k \left. \frac{\partial T_s(x, z)}{\partial z} \right|_{z=H}, \quad (9)$$

where  $k_k = k_s/k_f$  is defined as the ratio of the solid (boundary) heat conduction coefficient to the heat conduction coefficient of the flow.

In addition to the boundary conditions given by Eqs. (7) and (9), forced heat transfer convection is imposed at the boundary wall exterior surfaces, such that the heat flux through the boundary walls is governed by the following condition:

$$-k_s \left. \frac{\partial T_s(x, z)}{\partial z} \right|_{z=\bar{W}} = h[T_s(x, \bar{W}) - T_\infty], \quad 0 \leq x, \quad (10)$$

where  $T_\infty$  is the ambient temperature and  $h$  is the forced convection heat transfer coefficient.

*Non-Dimensional Equations*

It is customary to solve thermo-fluid problems after converting the governing equations and the corresponding boundary conditions into a non-dimensional form. The non-dimensional parameters used in this study are defined as follows:

$$U = \frac{u}{u_0}, \quad u_0 = \frac{1}{\mu} \left| \frac{\partial p}{\partial x} \right| H^2, \quad Z = \frac{z}{H}, \quad X = \frac{x}{H}, \quad t = \frac{\bar{t}}{H}, \quad W = \frac{\bar{W}}{H}, \quad \theta = \frac{T - T_\infty}{T_i - T_\infty}. \quad (11)$$

Accordingly, the equations from the previous section are rewritten in the non-dimensional form:

$$\frac{\partial^2 U}{\partial Z^2} = -1, \quad 0 < Z < 1, \quad 0 < X, \quad (12)$$

$$U \frac{\partial \theta_f}{\partial X} = \frac{1}{Pe} \frac{\partial^2 \theta_f}{\partial Z^2}, \quad 0 < Z < 1, \quad 0 < X, \quad (13)$$

$$\frac{\partial^2 \theta_s}{\partial Z^2} = 0, \quad 1 < Z < W, \quad 0 < X, \quad (14)$$

where  $Pe$  is the Peclet number, defined as  $Pe = u_0 H / \alpha$ ,  $\theta_f$ , and  $\theta_s$  are the temperature distributions in the fluid spatial domain  $0 < Z < 1$  and the solid-boundary spatial domain  $1 < Z < W$  respectively.

Similarly, the corresponding boundary conditions are presented below:

$$\frac{\partial U(Z)}{\partial Z} \Big|_{Z=0} = 0, \quad U(1) = -\beta_v Kn \frac{\partial U(Z)}{\partial Z} \Big|_{Z=1}, \quad (15, a, b)$$

$$\frac{\partial \theta_f(X, Z)}{\partial Z} \Big|_{Z=0} = 0, \quad (16)$$

$$\frac{\partial \theta_f(X, Z)}{\partial Z} \Big|_{Z=1} = k_k \frac{\partial \theta_s(X, Z)}{\partial Z} \Big|_{Z=1}, \quad \theta_f(X, 1) - \theta_s(X, 1) = -\beta_T Kn \frac{\partial \theta_f(X, Z)}{\partial Z} \Big|_{Z=1}, \quad (17)$$

$$\frac{\partial \theta_s(X, Z)}{\partial Z} \Big|_{Z=W} = -Bi \theta_s(X, Z) \Big|_{Z=W}. \quad (18)$$

In the last equations, the constant  $Kn = \lambda / H$  is the so called Knudsen number and  $Bi = h H / k_s$  is the Biot number of the exterior surface, based on the height  $H$  and the solid wall conduction coefficient  $k_s$ .

The fluid enters the channel with a uniform temperature higher than the ambient temperature, such that,

$$\theta_f(0, Z) = 1. \quad (19)$$

*Analytic Solution*

Eqs. (11)–(18) are a homogeneous set of coupled linear partial differential equations of variable coefficients and the associated boundary conditions. The flow condition at the channel entrance is given by Eq. (19).

The velocity profile of the flow is obtained by integrating Eq. (12) while the integration constants are determined by Eqs (15a, b). The integration result is

$$U(Z) = \frac{1}{2}(1 + 2Kn\beta_v - Z^2), \quad 0 < Z < 1, \quad 0 < X, \quad (20)$$

where the slip velocity at the solid–fluid interface is  $U_s = Kn\beta_v$ . Similarly, the temperature distribution  $\theta_s$  in the plates is obtained by integrating Eq. (14) twice and using Eq. (18) to obtain one of the integration constants. The integration yields that

$$\theta_s(X, Z) = \left( Z - W - \frac{1}{Bi} \right) C(X), \quad 1 < Z < W, \quad 0 < X. \quad (21)$$

The integration constant  $C(X)$  is not determined yet. Its expression depends on both the solid–fluid interfacial coupled boundary conditions given by Eq. (17) and the solution of the flow temperature distribution  $\theta_f(X, Z)$ , which is to be determined in the next section.

*Method of Separation of Variables*

The rarefied gas flow field temperature distribution is governed by Eq. (13) and its boundary conditions are described by Eqs. (16)–(19). The method of separation of variables can be used to obtain the analytic solutions. Let the solution  $\theta_f$  be written as the product of two functions  $g(X)$  and  $\mathfrak{R}(Z)$  such that

$$\theta_f(X, Z) = g(X) \cdot \mathfrak{R}(Z), \quad (22)$$

Substitution of  $\theta_f$  into Eqs. (13) and (16) yields the following homogenous ordinary differential equations:

$$\frac{dg(X)}{dX} = -\kappa^2 g(X), \quad (23)$$

where  $\kappa^2$  is constant, and

$$\frac{d^2\mathfrak{R}(Z)}{dZ^2} + \kappa^2 Pe U(Z) \mathfrak{R}(Z) = 0, \quad (24)$$

as well as the corresponding boundary conditions,

$$\left. \frac{d\mathfrak{R}(Z)}{dZ} \right|_{Z=0} = 0, \quad (25)$$

$$g(X) \cdot \mathfrak{R}(1) - \left[ (1 - W) - \frac{1}{Bi} \right] C(X) = -\beta_T Kn g(X) \left. \frac{d\mathfrak{R}(Z)}{dZ} \right|_{Z=1}, \quad (26)$$

$$\frac{1}{k_k} g(X) \left. \frac{d\mathfrak{R}(Z)}{dZ} \right|_{Z=1} = C(X). \quad (27)$$

Elimination of  $C(X)$  from the last two equations leads to the homogenous boundary condition,

$$\Re(1) - \left( \frac{1-W}{k_k} - \frac{1}{k_k Bi} - \beta_T Kn \right) \frac{d\Re(Z)}{dZ} \Big|_{Z=1} = 0. \quad (28)$$

With  $PeU(Z) > 0$  in the flow domain,  $0 \leq Z \leq 1$ , Eqs. (24), (25), and (28) correspond to the typical Sturm–Liouville problem. Its solution can be obtained by the eigenfunction expansion method. However, the use of transformation of variables defined by  $q = Z^2\sqrt{\bar{a}}$  and  $\psi = e^{q/2} \Re$  transforms Eq. (24) to a degenerate hypergeometric equation [37, 38], which is also called Kumar's equation:

$$q \frac{d^2\psi(q)}{dq^2} + (b-q) \frac{d\psi(q)}{dq} - a\psi(q) = 0, \quad 0 < q < \sqrt{\bar{a}}, \quad (29)$$

in which  $\bar{a}(\kappa) = \frac{\kappa^2 Pe}{2}$ ,  $a = \frac{1}{4} \left( \frac{\bar{b}}{\sqrt{\bar{a}}} + 1 \right)$ ,  $b = \frac{1}{2}$ ,  $\bar{b} = \kappa^2 Pe A$ , and  $A = \frac{1}{2} + Kn \beta_v$ .

Furthermore, Eqs. (25) and (28) transform to

$$\frac{d\psi(q)}{dq} \Big|_{q=0} = 0, \quad (30a)$$

$$\psi(\sqrt{\bar{a}}) - \left[ \frac{1-W}{k_k} - \frac{1}{k_k Bi} - \beta_T Kn \right] [-\psi(\sqrt{\bar{a}}) + 2\psi'(\sqrt{\bar{a}})]\sqrt{\bar{a}} = 0. \quad (30b)$$

The homogeneous solutions of Eq. (29) are given by Kummer's functions defined by the series form:

$$\phi(q; a, b) = 1 + \sum_{n=1}^{\infty} \frac{(a)_n q^n}{(b)_n n!}, \quad (31a)$$

$$M(q; a, b) = q^{1-b} \phi(q; a-b+1, 2-b), \quad (31b)$$

The Pochhammer function  $(a)_n$  is defined as follows [38]:

$$(a)_n = a(a+1)(a+2) \dots (a+n-1) = \frac{\Gamma(a+n)}{\Gamma(a)}, \quad (32)$$

where  $\Gamma$  is the well-known Gamma function. With these solutions, the general solution  $\psi$  of Eq. (29) is the following linear combination:

$$\psi = C_1 \phi + C_2 M. \quad (33)$$

Application of the symmetrical boundary conditions of Eq. (30a) eliminates the second solution  $C_2 = 0$ , and implementation of the second boundary condition imposed by Eq. (30b) leads to the characteristic equation

$$\phi(\sqrt{\bar{a}}; a, b) + \sqrt{\bar{a}} \left[ \frac{1 + Bi(W-1)}{k_k Bi} + \beta_T Kn \right] \left[ 2\phi'(\sqrt{\bar{a}}; a, b) - \phi(\sqrt{\bar{a}}; a, b) \right] = 0. \quad (34)$$

Here the derivative of  $\phi$  is given by [38],

$$\frac{d^n}{dq^n} \phi(q; a, b) = \frac{(a)_n}{(b)_n} \phi(q; a+n, b+n). \quad (35)$$



The left-hand-side of Eq. (34) is implicitly a function of the constant  $\kappa$  since  $\bar{a}$ ,  $a$ , and  $b$  are defined in terms of  $\kappa$ . The solution of this equation provides values of the eigenvalues  $\kappa_1^2, \kappa_2^2, \kappa_3^2, \dots, \kappa_\infty^2$  and the corresponding eigenfunctions  $\phi_1, \phi_2, \phi_3, \dots, \phi_\infty$ . Consequently, the solutions of Eqs. (23) and (24) are respectively given by the following:

$$g_i(X) = D_i e^{-\kappa_i^2 X}, \quad i = 1, 2, 3, \dots, \infty, \quad (36)$$

$$\mathfrak{R}_i(Z) = \phi_i \left( \sqrt{\bar{a}} Z^2; a, b \right) e^{-\frac{\sqrt{\bar{a}}}{2} Z^2}, \quad i = 1, 2, 3, \dots, \infty. \quad (37)$$

Therefore, the flow temperature profile  $\theta_f$  can be written in the indefinite series form as

$$\theta_f(X, Z) = \sum_{i=1}^{\infty} D_i e^{-\kappa_i^2 X + \frac{\sqrt{\bar{a}}}{2} Z^2} \phi_i \left( \sqrt{\bar{a}} Z^2; a, b \right), \quad 0 < Z < 1, \quad 0 < X. \quad (38)$$

The use of the orthogonality property of the eigenfunctions and the entrance value of  $\theta_f$  given by Eq. (19) yield the values of constants  $D_i$ , where

$$D_i = \frac{\int_0^1 U(Z) e^{-\frac{\sqrt{\bar{a}}}{2} Z^2} \phi_i \left( \sqrt{\bar{a}} Z^2; a, b \right) dZ}{\int_0^1 U(Z) \left( e^{-\frac{\sqrt{\bar{a}}}{2} Z^2} \phi_i \left( \sqrt{\bar{a}} Z^2; a, b \right) \right)^2 dZ}. \quad (39)$$

Recalling Eq. (27), the constant of integration  $C(X)$  can now be written as

$$C(X) = \frac{1}{k_k} \frac{\partial \theta_f}{\partial Z} \Big|_{Z=1}. \quad (40)$$

Hence, the temperature distribution  $\theta_s$  given by Eq. (21) is recast as follows:

$$\theta_s(X, Z) = - \left( \frac{W - Z}{k_k} + \frac{1}{k_k Bi} \right) \frac{\partial \theta_f}{\partial Z} \Big|_{Z=1}, \quad 1 < Z < W, \quad 0 < X. \quad (41)$$

The microchannel flow local Nusselt number can be derived as follows:

$$h_f (T_w - T_m) = \frac{k_f}{H} \frac{\partial \theta_f}{\partial Z} \Big|_{Z=1} (T_i - T_\infty), \quad (42)$$

$$Nu = \frac{h_f H}{k_f} = \frac{1}{[(T_w - T_\infty) - (T_m - T_\infty)] / (T_i - T_\infty)} \frac{\partial \theta_f}{\partial Z} \Big|_{Z=1} = \frac{1}{(\theta_w - \theta_m)} \frac{\partial \theta_f}{\partial Z} \Big|_{Z=1}, \quad (43)$$

where  $T_w$  is the temperature of the fluid at the inner surface of the boundary wall,  $h_f$  is the microchannel flow local convection heat transfer coefficient, and  $\theta_m$  is the mean local bulk temperature of the flow, defined by the relation

$$\theta_m = \frac{\int_0^1 U \theta_f dZ}{\int_0^1 U dZ}. \quad (44)$$

However, it is customary to define the Nusselt number in terms of the hydraulic diameter  $D_h$  of the flow. Accordingly, the Nusselt number can be redefined as

$$Nu = 4 \frac{h_f H}{k_f},$$

where the hydraulic diameter of the semi-infinite parallel plates channel is  $D_h = 4H$ .

## RESULTS AND DISCUSSION

The number of physical parameters involved in the formulation of the problem is large. Therefore, unless otherwise mentioned, the results presented in this section are based on the values of predefined base-line parameters. These values are the momentum and the thermal accommodation factors ( $\sigma_v = \sigma_T = 0.8$ ), the Knudsen number ( $Kn = 0.05$ ), the Peclet number ( $Pe = 5$ ), the Prandtl number ( $Pr = 0.75$ ), the heat transfer conductivity ratio ( $k_k = 3$ ), the Biot number ( $Bi = 2$ ), and the wall thickness ( $t = 0.4$ ).

The eigenvalues of the solutions presented in this section are obtained by solving Eq. (34) using a mathematical solver software package. For brevity, the table lists only the six significant digits of the numerical values of the first six eigenvalues used to obtain the solutions of Fig. 10 (see below).

The analytic solutions were verified by comparison with available data in the literature. For example, it is found that the Nusselt number values based on the obtained solutions are in perfect match with the Nusselt number values corresponding to well-known solutions in the literature, such as the unconjugated conventional semi-infinite parallel-plate flow of either isothermal or constant heat flux boundary walls. In this study, the unconjugated conventional heat transfer was simulated by setting the wall thickness ( $t \approx 0$ ) and the Knudsen number ( $Kn \approx 0$ ). In addition, the Biot number was assigned a large value ( $Bi > 100$ ) to have a flow of isothermal boundary condition or a small value ( $Bi < 0.1$ ) in order to have a flow of adiabatic boundaries, which is a special case of constant heat flux boundary conditions ( $q'' = 0$ ). Figure 2 presents the fully developed values of the Nusselt number for the isothermal and adiabatic boundary cases, 7.56 and 8.22, respectively. Both values agree well with the values available in [39].

Figure 3 represents the evolution of the temperature solutions  $\theta$  at different axial locations. Since it is losing its energy content, the temperature  $\theta$  decays as the fluid flows streamwise and attains the value of the ambient temperature at the downstream location  $X \approx 8$  where the temperature  $\theta = 0$ . According to the conductivity ratio ( $k_k = 3$ ), the flow field temperature gradient  $d\theta_f/dZ$  in the vicinity of the solid-fluid interface is always higher than its value within the boundary wall ( $d\theta_f/dZ > d\theta_s/dZ$ ). Both gradients decay streamwise and vanish as the flow passes the axial position  $X \approx 8$ . The difference  $\Delta\theta = \theta_f(X, 1) - \theta_s(X, 1)$  is the temperature jump at the fluid solid interface, as it was anticipated; the fluid enters the channel with the maximum temperature-jump  $\Delta\theta$  and decays streamwise.

The conduction heat transfer ratio  $k_k$  is a key parameter that defines the thermal behavior of the system with two limiting cases. The  $k_k$  values used to get solutions of Fig. 4 fall between these limiting

Values of the first six eigenvalues ( $\kappa$ ) of solutions of Fig. 10

| $Pe$ | $\kappa_1$ | $\kappa_2$ | $\kappa_3$ | $\kappa_4$ | $\kappa_5$ | $\kappa_6$ |
|------|------------|------------|------------|------------|------------|------------|
| 1    | 1.650642   | 6.220670   | 11.010831  | 15.883293  | 20.798774  | 25.740011  |
| 2    | 1.167180   | 4.398678   | 7.785833   | 11.231184  | 14.706954  | 18.200936  |
| 3    | 0.952998   | 3.591505   | 6.357106   | 9.170223   | 12.008178  | 14.861003  |
| 4    | 0.82532    | 3.110335   | 5.505415   | 7.941647   | 10.399387  | 12.870006  |
| 5    | 0.673872   | 2.539578   | 4.495153   | 6.4843273  | 8.491064   | 10.508316  |
| 10   | 0.521979   | 1.967149   | 3.481930   | 5.022738   | 6.57715    | 8.139706   |
| 15   | 0.426194   | 1.606170   | 2.842984   | 4.101048   | 5.370220   | 6.646042   |

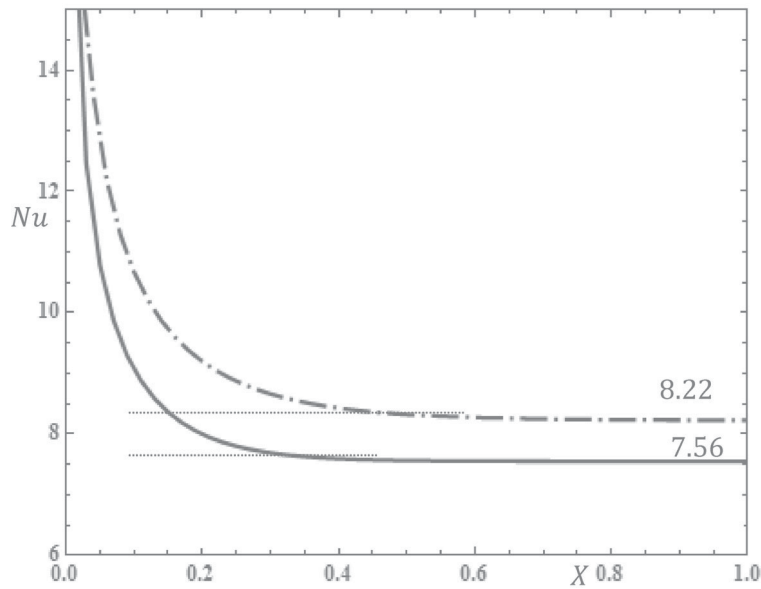


Fig. 2. Nusselt number values for conventional unjugated heat transfer.

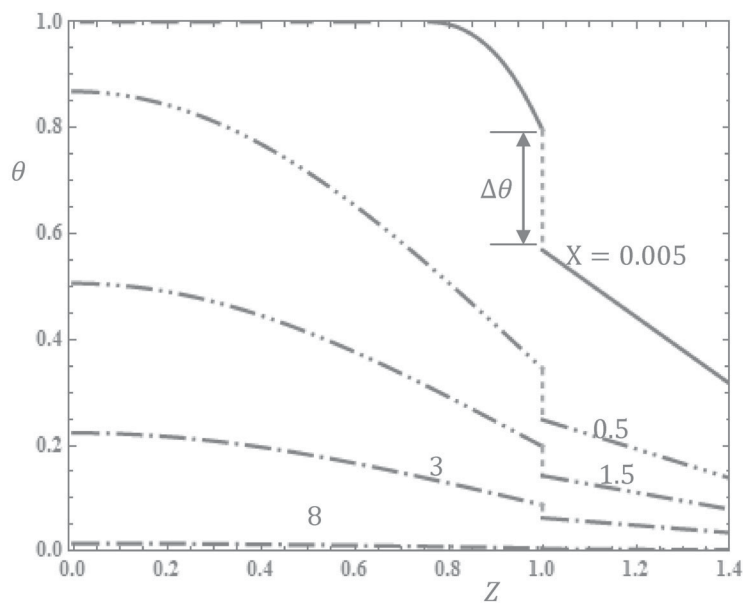


Fig. 3. Thermal entrance region temperature distributions for values of base-line parameters.

values. For large  $k_k$  ( $k_k = 100$ ), the heat conduction through the wall exceeds by far the heat transfer through the flow adjacent to the wall inner surface. Hence, the wall temperature attains an isothermal boundary limit ( $\theta_s = 0$ ) whereas the fluid temperature distribution is parabolic. In addition, for  $k_k$  of about 100 it is found that the temperature jump is relatively the highest, as shown in Fig. 4. On contrary, an adiabatic wall limiting case can be approached with small values of  $k_k$  approximately equal to zero. In this case, the heat conduction through the boundary wall is very weak, and the external surface of the boundary attains the ambient temperature, while its internal surface gets that of the microchannel flow. Therefore, the temperature gradient through the wall is of the largest possible value, and the microchannel-flow field temperature distribution is uniform.

It is also shown in Fig. 4 that the temperature distribution  $\theta$  decays as  $k_k$  increases. Furthermore, as shown in Fig. 5, the temperature jump  $\Delta\theta = (\theta_f - \theta_s)|_{Z=1}$  equals to zero for all axial locations when

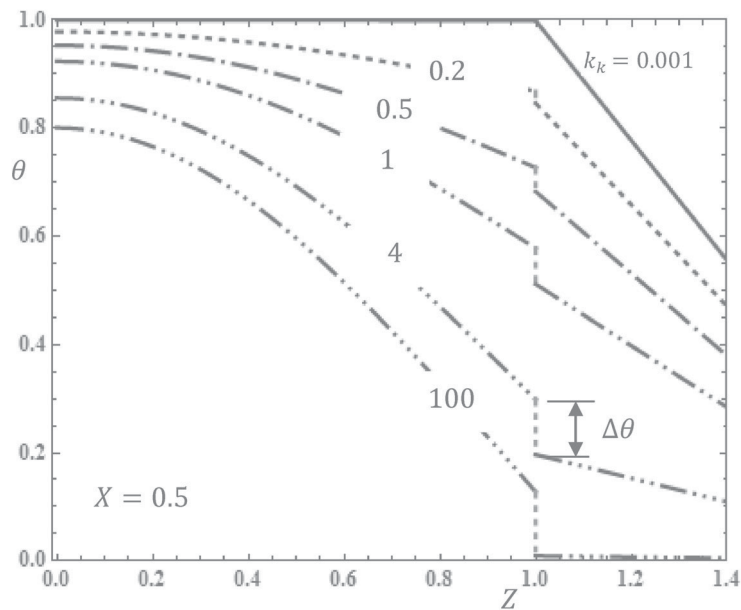


Fig. 4. Temperature distributions in entrance region for various values of  $k_k$ .

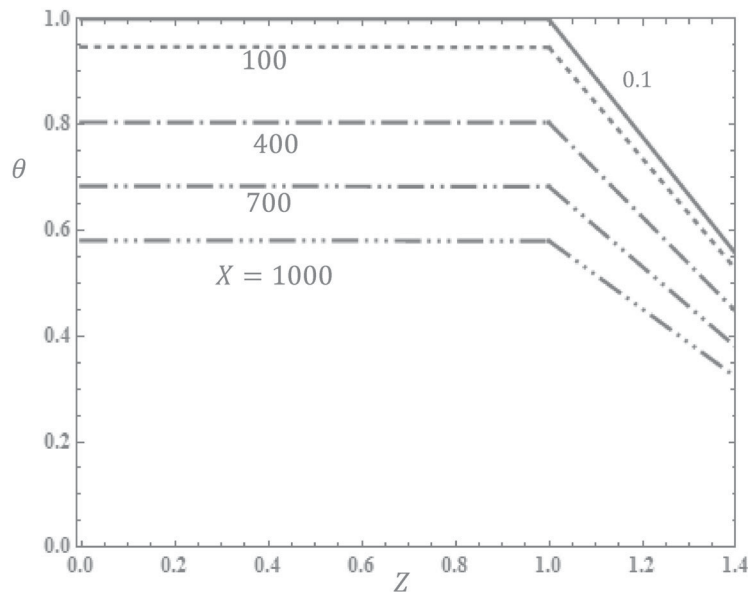


Fig. 5. Evolution of temperature distributions in axial direction for small  $k_k$ .

$k_k \approx 0$ . The temperature solution presented in Fig. 6 shows decaying temperature profiles at different transverse locations in the streamwise direction. The earlier-defined temperature jump  $\Delta\theta$  appears in Fig. 6 as the difference between the temperature curves  $\theta_f$  and  $\theta_s$  of the fluid and the solid boundary, respectively, at the solid-fluid interface ( $Z = 1$ ).

The Knudsen number is an influential parameter pertinent to microchannel-flow problems. Figure 7 presents the transverse temperature distribution at the axial location ( $X = 0.1$ ). It is shown that the effect of  $Kn$  on the temperature solution is more pronounced in the fluid domain ( $0 < Z < 1$ ) than in the solid domain ( $1 < Z < 1.4$ ). It is also shown that  $\theta_f$  increases with the Knudsen number, whereas in the solid domain  $\theta_s$  follows the opposite trend. The strongest solid-fluid interfacial hydrodynamic and thermal coupling, characterized by  $Kn < 0.001$ , represents the case of macro-fluid flow, where the

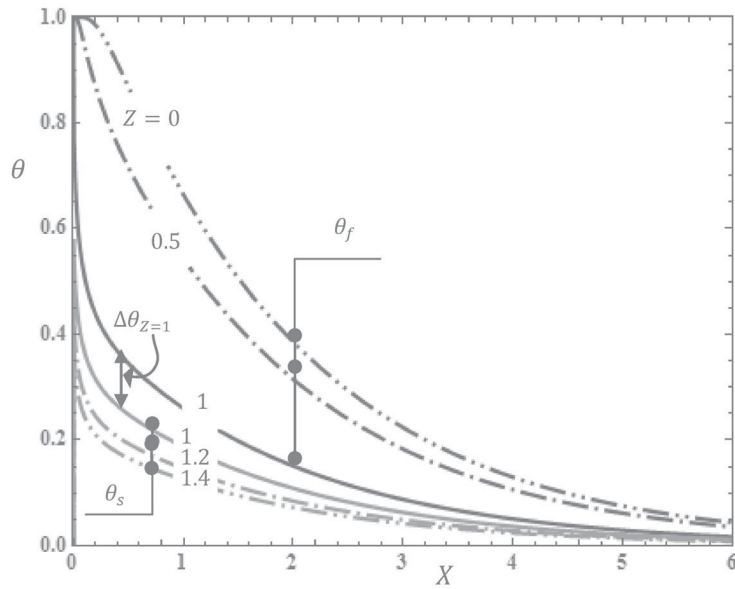


Fig. 6. Axial temperature distributions at different lateral locations  $Z$ .

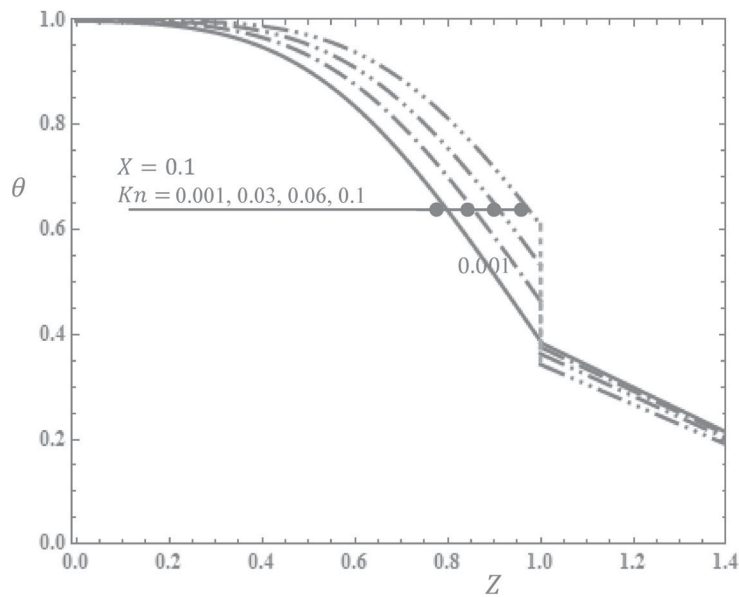


Fig. 7. Effect of  $Kn$  on  $\theta$  at two different downstream locations for  $X = 0.1$ .

interfacial temperature jump is zero. However, the increase in  $Kn$  relaxes the interfacial thermal coupling constraint, and therefore the fluid flow temperature  $\theta_f$  driven by the prescribed entrance temperature value, grows with  $Kn$ . On the other hand, the boundary wall temperature  $\theta_s$  driven by the prescribed Biot number of the external surface and ambient temperature, decreases as  $Kn$  increases.

Figure 8 presents the effect of the thermal accommodation factor  $\sigma_T$  on the temperature distribution. The value of  $\sigma_T$  controls the amount of heat energy that can cross the solid–fluid interface. For small accommodation factor values,  $\sigma_T \approx 0$ , molecular collisions with the solid boundary are almost specular, and hence the energy content of the flow is almost preserved and the flow retains its uniform temperature distribution ( $\theta_f = 1$ ) and the temperature of the boundary wall remains equal to the ambient temperature ( $\theta_s = 0$ ). This situation ideally represents an unconjugated heat transfer problem with insulating boundaries. On the other hand, with larger values of accommodation factors, part of the energy content

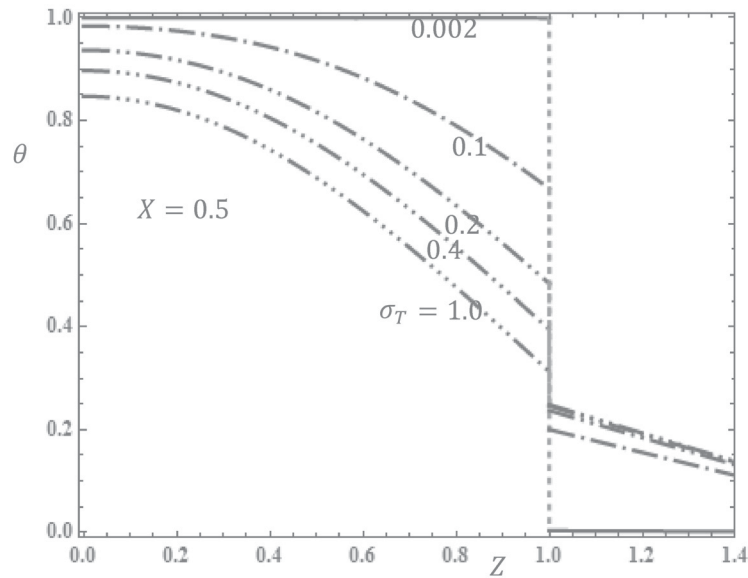


Fig. 8. Effect of  $\sigma_T$  on  $\theta$  at downstream location for  $X = 0.5$ .

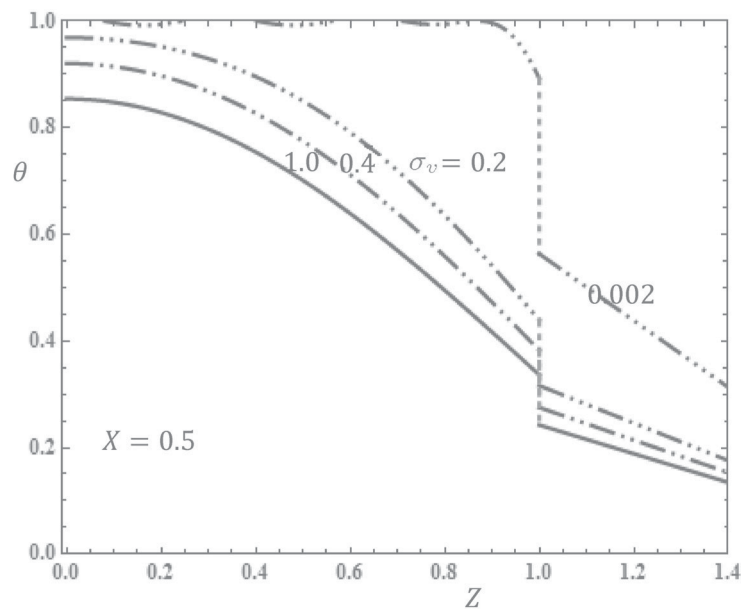


Fig. 9. Effect of  $\sigma_v$  on  $\theta$  at downstream location for  $X = 0.5$ .

of the flow will be exchanged with the boundary walls via diffuse molecular collisions, and hence the flow field temperature becomes lower and the boundary wall temperature gets larger. Figure 9 portrays the effect of the momentum accommodation factor  $\sigma_v$ . Figure 10 demonstrates the effect of the Peclet number  $Pe$  on the temperature solution. It is clearly shown that the temperature distributions of both the fluid and solid domains increase monotonically with  $Pe$ .

However, the temperature profiles become less sensitive to the change in the Peclet number  $\Delta Pe$  as  $Pe$  attains large values. Similarly, Fig. 11 shows the effect of the Prandtl number  $Pr$  on the solution. Here, the temperature solution is found to be inversely proportional to the Prandtl number in the fluid domain and directly proportional to the Prandtl number in the solid domain. From another aspect, it is found that the effect of the Prandtl number on the temperature distributions is more pronounced in the fluid flow domain.

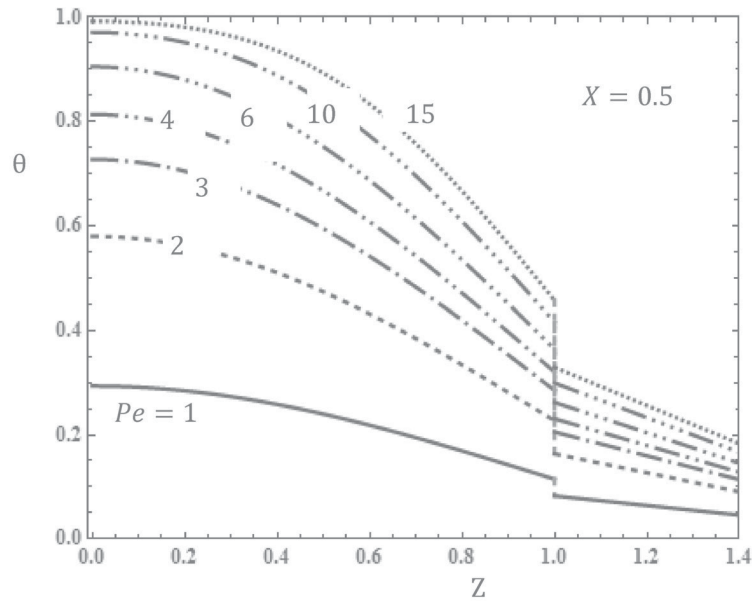


Fig. 10. Effect of  $Pe$  on  $\theta$  at downstream location for  $X = 0.5$ .

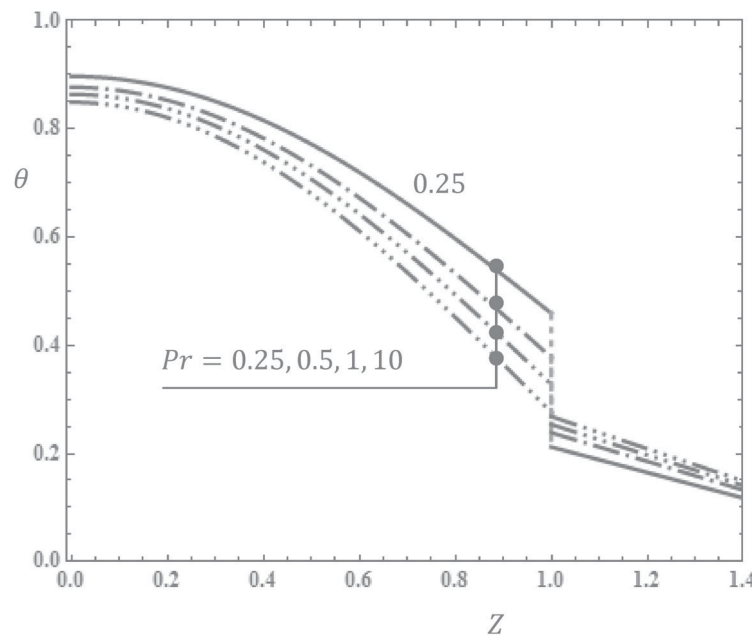


Fig. 11. Effect of  $Pr$  on  $\theta$  at downstream location for  $X = 0.5$ .

The temperature jump  $\Delta\theta$  at the solid-fluid interface is the key result that differentiates the classical macro scale fluid flow and the corresponding micro scale one. The effects of the  $Kn$ ,  $Bi$ , and  $k_k$  on  $\Delta\theta$  are demonstrated for different axial locations  $X$  in Figs. 12, 13, and 14, respectively. As seen in Fig. 12, the temperature jump curves are almost linear functions of  $Kn$  for all considered axial locations. The slope of these curves diminishes as the flow proceeds downstream. Figures 13 and 14 are semi-log plots that demonstrate the effect of both  $Bi$  and  $k_k$  on the temperature solution, respectively. It is shown that both parameters have qualitatively similar effect on the thermal solution as both  $Bi$  and  $k_k$  control the quantity of heat that can pass through the boundary walls. Accordingly, increase in the value of  $Bi$  and/or  $k_k$  leads to increase in the temperature jump  $\Delta\theta$  at the solid-fluid interface, which is found to asymptotically approach a fixed value at each considered axial location.

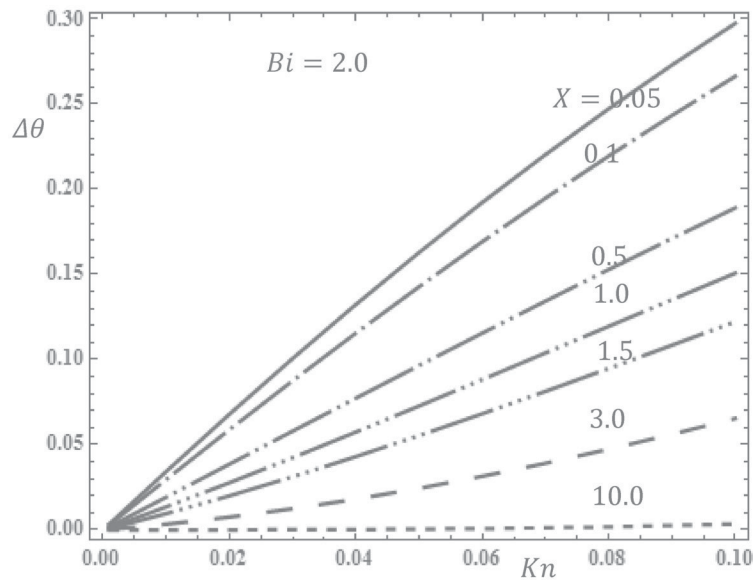


Fig. 12. Effect of  $Kn$  on solid-fluid interface temperature jump at different axial locations.

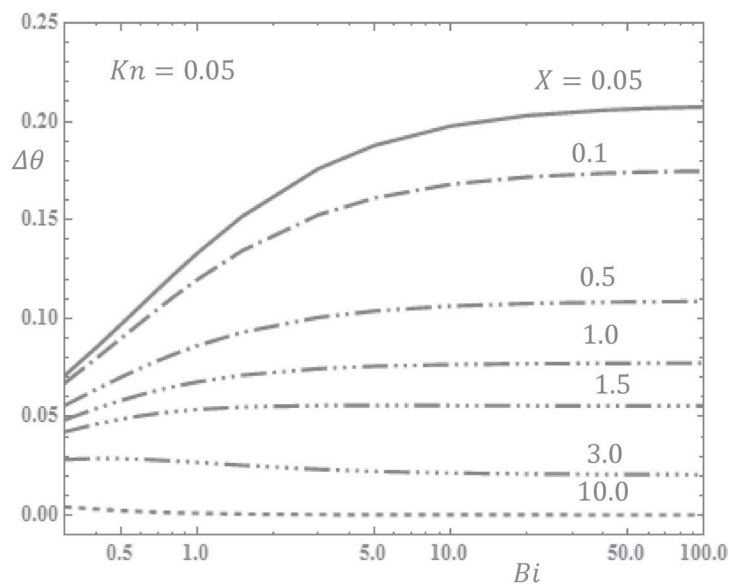


Fig. 13. Effect of  $Bi$  on solid-fluid interface temperature jump at different axial locations.

The Nusselt number  $Nu$  is another parameter pertinent to the heat transfer phenomena. Figures 15, 16, and 17 represent the effect of  $Kn$ ,  $k_k$ , and  $Bi$ , respectively, on the Nusselt number axial distribution. Figure 15 reveals that  $Nu$  grows with  $Kn$ . This reflects a more pronounced tendency of the flow to transfer the heat via the convection mode as compared with the conduction mode. From another point of view, the large values of  $Nu$  near the entrance region are due to the large values of the temperature difference  $\theta_w - \theta_m$ , which means domination of the convection heat transfer mode. As the fluid flows downstream, the temperature difference  $\theta_w - \theta_m$  decreases; therefore,  $Nu$  decays and tends asymptotically to the thermally fully developed value,  $Nu \approx 7.8$  for  $Kn = 0.001$ . Figure 16 shows the effect  $k_k$  on  $Nu$ , which is found to have a trend opposite to the trends observed in Fig. 15. As  $k_k$  increases, the conduction heat transfer mode in the solid boundaries becomes more significant since more heat can pass through and thus  $Nu$  decreases monotonically as  $k_k$  increases. In a similar fashion, Fig. 17 shows that the Nusselt number decreases monotonically as the Biot number grows. Finally, the



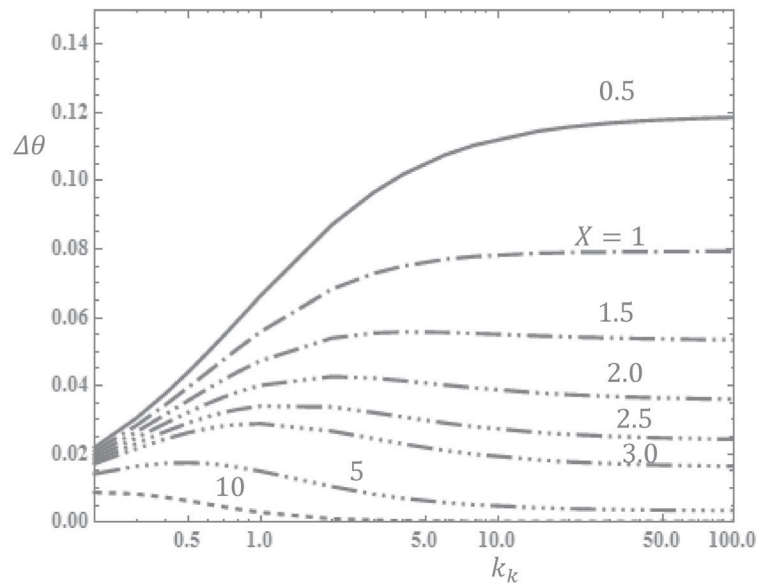


Fig. 14. Effect of  $k_k$  on solid-fluid interface temperature jump at different axial locations.

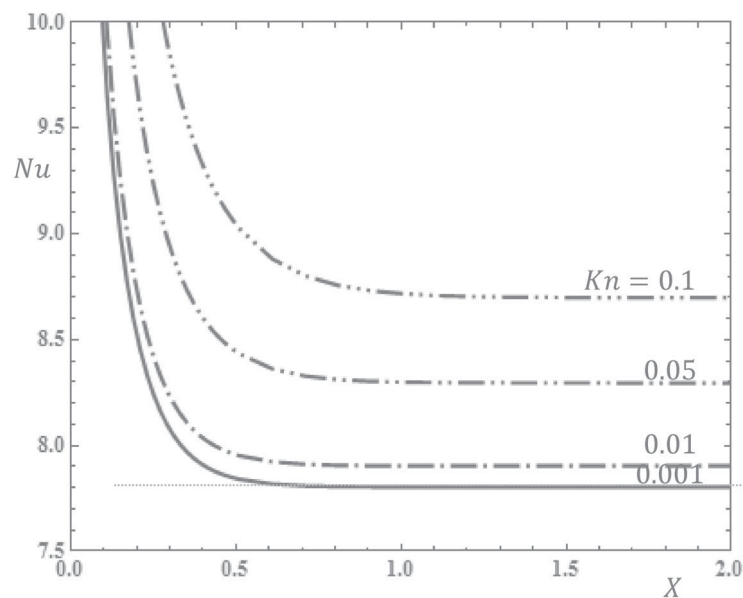


Fig. 15. Nusselt number for different values of  $Kn$ .

effect of the wall thickness on the thermal solution is presented in Fig. 18 in the form of two solution bundles corresponding to two values of the Knudsen number:  $Kn \approx 0.001$  and  $0.1$ . In both cases, it is shown that increase in the wall thickness leads to rise in the Nusselt number. This is due to larger wall thermal resistance, which in turn leads to a drop in the conduction heat transfer through the boundaries and subsequently to greater values of the Nusselt number.

## CONCLUSIONS

The conjugated heat transfer problem of rarified gas flow between parallel micro plates has been addressed analytically. The flow was considered to be subjected to forced convection that was characterized by the Biot number at the external surfaces of the boundary walls. The standard method

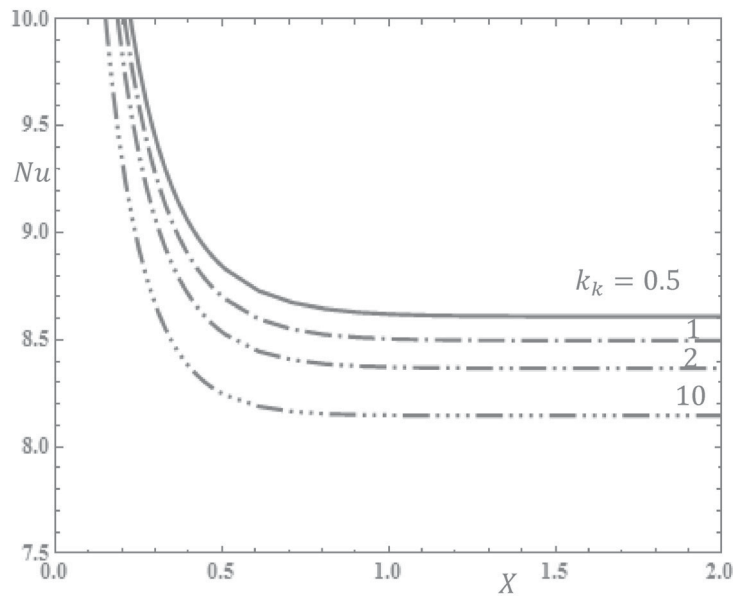


Fig. 16. Nusselt number for different values of  $k_k$ .

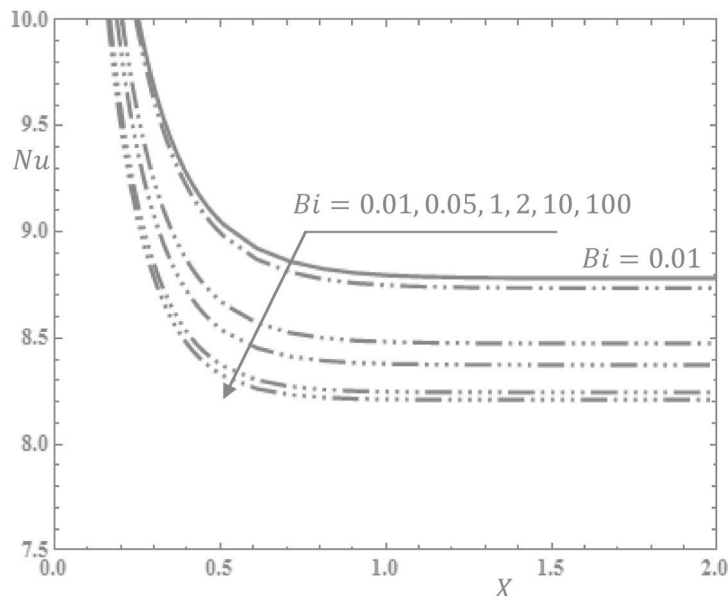


Fig. 17. Nusselt number for different values of  $Bi$ .

of separation of variables was used to split the non-dimensional energy equation into two ordinary differential equations. One of these differential equations corresponded to the canonical form of the Sturm-Liouville problem, which in turn was transformed to a degenerate hypergeometric differential equation. The solutions of the degenerate hypergeometric differential equation were given in terms of Kummer's functions. The application of the boundary conditions led to a transcendental characteristic equation. The eigenvalues of the problem or the roots of the characteristic equation were determined using a mathematical solver software package. The analytic values of  $Nu$  for special cases of both isothermal and constant heat flux boundaries agreed well with the data available in the literature. The effect of the problem key parameters on the thermal solutions was extensively investigated. The Nusselt number values were found to increase with the Knudsen number. Furthermore, the Nusselt number value was initially high near the flow inlet and decreased asymptotically to a constant value downstream.

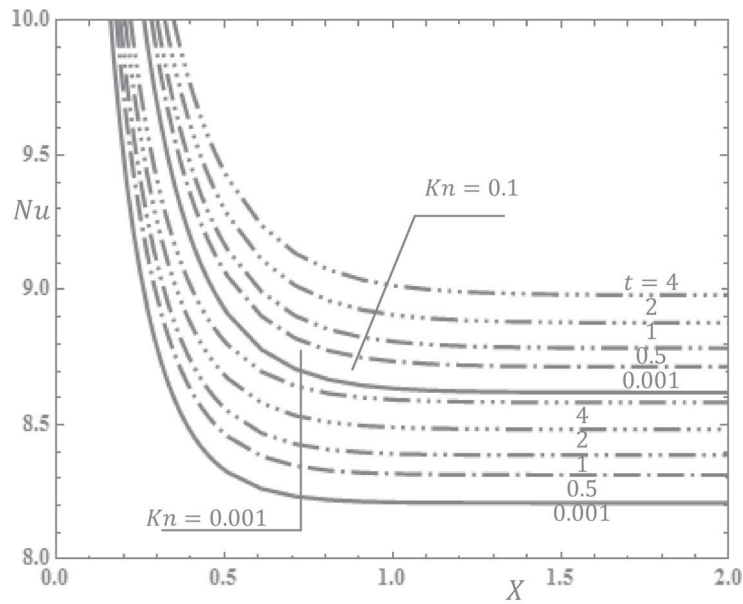


Fig. 18. Nusselt number for different values of boundary thickness  $t$ .

On contrary, the Nusselt number diminished with increase either in the Biot number or in the conduction ratio parameter. From another aspect, the effect of thicker solid boundary on the thermal solution was found to be similar to the effect of decrease in the value of the conduction ratio or the Biot number. Finally, the temperature jump at the fluid-solid interface was found to grow almost linearly with the Knudsen number for all axial locations near the entrance region ( $X < 10$ ) and to vanish downstream. In general, the temperature jump at the interface increased with either the Biot number or the heat conduction ratio before it reached an asymptotic value for each axial location.

#### NOTATIONS

- $A$ — $(\frac{1}{2} + Kn \beta_v)$ , constant  
 $a$ — $\frac{1}{4} \left( \frac{\bar{b}}{\sqrt{a}} + 1 \right)$ , constant  
 $\bar{a}(\kappa)$ — $\frac{\kappa^2 Pe}{2}$ , constant,  $\text{Pa}^2 \text{s}^2$   
 $(a)_n$ — $\frac{\Gamma(a+n)}{\Gamma(a)}$ , Pochhammer function  
 $Bi$ — $h H/k_s$ , the Biot number of the exterior surface  
 $b$ —constant (= 0.5)  
 $\bar{b}$ — $\kappa^2 Pe A$ , constant,  $\text{Pa}^2 \text{s}^2$   
 $C(X)$ —partial integration constant  
 $c$ —specific heat,  $\text{J}/(\text{kg} \cdot ^\circ\text{C})$   
 $D_i$ —constant  
 $H$ —half of channel depth, m  
 $h$ —heat convection coefficient with ambient,  $\text{J}/(\text{m}^2 \cdot \text{K})$   
 $h_f$ —heat convection coefficient of internal flow,  $\text{J}/(\text{m}^2 \cdot \text{K})$   
 $Kn$ —the Knudsen number  
 $k$ —thermal conductivity,  $\text{W}/(\text{m} \cdot \text{K})$   
 $k_k$ — $k_s/k_f$ , heat conduction ratio  
 $Nu$ —the Nusselt number  
 $Pe$ —the Peclet number

$Pr$ —the Prandtl number  
 $p$ —static pressure, Pa  
 $\bar{t}$ —plate thickness, m  
 $t$ — $t \frac{\bar{t}}{H}$ , nondimensional plate thickness  
 $T$ —dimensional temperature, K  
 $U$ —nondimensional velocity  
 $u$ —velocity, m/s  
 $u_0$ — $\frac{1}{\mu} \left| \frac{\partial p}{\partial x} \right| H^2$ , reference velocity, m/s  
 $W$ — $W \frac{\bar{W}}{H}$ , nondimensional channel half height  
 $X, Z$ —nondimensional rectangular coordinates

### Greek Symbols

$\beta_T$ —thermal accommodation coefficient  
 $\Gamma$ —gamma function  
 $\gamma$ —specific heat ratio  
 $\theta$ —nondimensional temperature  
 $\lambda$ —molecular mean free path  
 $\mu$ —viscosity  
 $\kappa$ —eigenvalue  
 $\rho$ —density, kg/m<sup>3</sup>  
 $\sigma_v$ —tangential momentum accommodation factor  
 $\sigma_T$ —thermal accommodation factor  
 $\phi_i$ — $i$ th eigenfunction

### Subscripts

$T$ —thermal  
 $v$ —tangential momentum  
 $i$ —index number

### REFERENCES

1. Graetz, L., Über die Wärmeleitungsfähigkeit von Flüssigkeiten (On the Thermal Conductivity of Liquids), Part 1, *Ann. Phys. Chem.*, 1883, vol. 18, pp. 79–94.
2. Graetz, L., Über die Wärmeleitungsfähigkeit von Flüssigkeiten (On the Thermal Conductivity of Liquids), Part 2, *Ann. Phys. Chem.*, 1885, vol. 25, pp. 337–357.
3. Nusselt, W., Die abhängigkeit der wärmeübergangszahl von der Rohrlänge (The Dependence of the Heat Transfer Coefficient on the Tube Length), *VDI*, 1910, vol. Z54, pp. 1154–1158.
4. Shah, A.L.R.K., *Laminar Flow Forced Convection in Ducts: A Source Book for Compact Heat Exchanger Analytical Data*, Academic Press, 1978, pp. 78–138.
5. Mikhailov, M.D. and Cotta, R.M., Mixed-Symbolic Computation of Convective Heat Transfer with Slip Flow in Microchannels, *Int. Comm. Heat Mass Transfer*, 2005, vol. 32, pp. 341–384.
6. Jeong, H.E. and Jeong, J.T., Extended Graetz Problem Including Streamwise Conduction and Viscous Dissipation in Microchannel, *Int. J. Heat Mass Transfer*, 2006, vol. 49, pp. 2151–2157.
7. Aydın, O. and Avcı, M., Analysis of Micro-Graetz Problem in a Microtube, *Nanoscale Microscale Thermophys. Eng.*, 2006, vol. 10, pp. 345–358.
8. Çetin, B., Yazicioglu, A.G., and Kakaç, S., Slip-Flow Heat Transfer in Microtubes with Axial Conduction and Viscous Dissipation—An Extended Graetz Problem, *Int. J. Therm. Sci.*, 2009, vol. 48, pp. 1673–1678.
9. Aydın, O. and Avcı, M., Analysis of Laminar Heat Transfer in Micro-Poiseuille Flow, *Int. J. Therm. Sci.*, 2007, vol. 46, pp. 30–37.
10. Aydın, O. and Avcı, M., Heat and Fluid Flow Characteristics of Gases in Micropipes, *Int. J. Heat Mass Transfer*, 200, vol. 649, pp. 1723–1730.

11. Avci, M. and Aydın, O., Laminar Forced Convection Slip-Flow in a Micro-Annulus between Two Concentric Cylinders, *Int. J. Heat Mass Transfer*, 2008, vol. 51, pp. 3460–3467.
12. Lee, P. and Garimella, S.G., Thermally Developing Flow and Heat Transfer in Rectangular Microchannels of Different Aspect Ratios, *Int. J. Heat Mass Transfer*, 2006, vol. 49, pp. 3060–3067.
13. Kuddusi, L. and Egrican, N., Prediction of Heat Transfer Characteristics in Rectangular Microchannels for Slip Flow Regime and H1 Boundary Condition, *Int. J. Therm. Sci.*, 2005, vol. 44, pp. 513–520.
14. Kuddusi, L., Prediction of Temperature Distribution and Nusselt Number in Rectangular Microchannels at Wall Slip Condition for All Versions of Constant Wall Temperature, *Int. J. Therm. Sci.*, 2007, vol. 46, pp. 998–1010.
15. Kuddusi, L., and Cetegen, E., Prediction of Temperature Distribution and Nusselt Number in Rectangular Microchannels at Wall Slip Condition for All Versions of Constant Heat Flux, *Int. J. Heat Fluid Flow*, 2007, vol. 28, pp. 777–786.
16. Sadeghi, A. and Saidi, M.H., Second Law Analysis of Slip Flow Forced Convection through a Parallel Plate Microchannel, *Nanoscale Microscale Thermophys. Eng.*, 2010, vol. 14, pp. 209–228.
17. Baghani, M., Sadeghi, A., and Baghani, M., Gaseous Slip Flow Forced Convection in Microducts of Arbitrary but Constant Cross Section, *Nanoscale Microscale Thermophys. Eng.*, 2014, vol. 18, no. 4, pp. 354–372.
18. van Rij, J., Ameer, T., and Harman, T., The Effect of Viscous Dissipation and Rarefaction on Rectangular Microchannel Convective Heat Transfer, *Int. J. Therm. Sci.*, 2009, vol. 48, pp. 271–281.
19. Mahulikar, S.P., Gulhane, N.P., Pradhan, S.D., Hrisheekesh, K., and Prabhu, S.V., Pressure Drop Characteristics in Continuum-Based Laminar Compressible Microconvective Flow, *Nanoscale Microscale Therm. Eng.*, 2012, vol. 16, no. 3, pp. 181–197.
20. Morini, G.L., Analytical Determination of the Temperature Distribution and Nusselt Numbers in Rectangular Ducts with Constant Axial Heat Flux, *Int. J. Heat Mass Transfer*, 2000, vol. 43, no. 5, pp. 741–755.
21. Wang, X.S., Dagan, Z., and Jiji, L.M., Conjugated Heat Transfer between a Laminar Impinging Liquid Jet and a Solid Disk, *Int. J. Heat Mass Transfer*, 1989, vol. 32, pp. 2189–2197.
22. Olek, S., Unsteady Conjugated Heat Transfer in Laminar Pipe Flow, *Int. J. Heat Mass Transfer*, 1991, vol. 34, pp. 1450–1491.
23. Alnimer, A. and El-shaarawi, M.A.I., Analytical Solutions for Transient Conjugated Heat Transfer in Parallel Plate and Circular Duct, *Int. Comm. Heat Mass Transfer*, 1992, vol. 19, pp. 869–878.
24. Yan, W., Transient Conjugated Heat Transfer in Channel Flow with Convection from the Ambient, *Int. J. Heat Mass Transfer*, 1993, vol. 36, no. 5, pp. 1295–1301.
25. Bilir, S., Transient Conjugated Heat Transfer in Pipes Involving Two-Dimensional Wall and Axial Fluid Conduction, *Int. J. Heat Mass Transfer*, 2002, vol. 45, pp. 1781–1788.
26. Mathei, R. and Markides, C.N., Heat Transfer Augmentation in Unsteady Conjugate Thermal System, Part I: Semi-Analytical 1-D Framework, *Int. J. Heat Mass Transfer*, 2013, vol. 56, pp. 802–818.
27. Bilgen, E., Conjugated Heat Transfer by Conduction and Natural Convection on a Heated Vertical Wall, *Appl. Therm. Eng.*, 2009, vol. 29, pp. 334–339.
28. Juncu, G., Unsteady Conjugated Forced Convection Heat/Mass Transfer from a Finite Plate, *Int. J. Therm. Sci.*, 2008, vol. 47, pp. 972–984.
29. Pozzi, A. and Tognaccini, R., Conjugated Heat Transfer in Unsteady Channel Flows, *Int. J. Heat Mass Transfer*, 2011, vol. 54, pp. 4019–4027.
30. Machado, J.F.B. et al., A Simplified Model with a Hybrid Analytical-Numerical Solution for Predicting the Unsteady Conjugate Heat Transfer Process in Pipelines, Numerical Heat Transfer, Part B: Fundamentals, *Int. J. Comput. Methodol.*, 2011, vol. 60, pp. 18–33.
31. Ambatipudi, K.K. and Rahman, M.M., Analysis of Conjugate Heat Transfer in Microchannel Heat Sinks, *Num. Heat Transfer*, Part A, 2000, vol. 37, pp. 711–731.
32. Harms, T.M., Heat Transfer and Fluid Flow in Deep Rectangular Liquid-Cooled Microchannels Etched in a (110) Silicon Substrate, Master Thesis, University of Cincinnati, Cincinnati, OH, 1997.
33. Zhang, S.X., He, Y.L., Lauriat, G., and Tao, W.Q., Numerical Studies of Simultaneously Developing Laminar Flow and Heat Transfer in Microtubes with Thick Wall and Constant Outside Wall Temperature, *Int. J. Heat Mass Transfer*, 2010, vol. 53, pp. 3977–3989.
34. Nonino, C., Savino, S., Del Giudice, S., and Mansutti, L., Conjugate Forced Convection and Heat Conduction in Circular Microchannels, *Int. J. Heat Fluid Flow*, 2009, vol. 30, pp. 823–830.

35. Avci, M., Aydın, O., and Arıcı, M.E., Conjugate Heat Transfer with Viscous Dissipation in a Microtube, *Int. J. Heat Mass Transfer*, 2012, vol. 55, pp. 5302–5308.
36. Kabar, Y., Bessaih, R., and Rebay, M., Conjugate Heat Transfer with Rarefaction in Parallel Plates Microchannel, *Superlatt. Microstruct.*, 2013, vol. 60, pp. 370–388.
37. Polyanin, A.D. and Zaitsev, V.F., *Handbook of Exact Solutions for Ordinary Differential Equations*, 2nd ed., Chapman and Hall/CRC, 2002.
38. Abramowitz, M. and Stegun, I.A., *Handbook of Mathematical Functions With Formulas, Graphs and Mathematical Tables*, 1964.
39. Incropera, F.P., Dewitt, D. P., Bergman, T. L., and Lavine, A.S., *Fundamentals of Heat and Mass Transfer*, 2nd ed., Wiley, 2007.